Ferric heme as a CO/NO sensor in the nuclear receptor Rev-Erbß by coupling gas binding to electron transfer

Anindita Sarkar[a], Eric L. Carter[a,1], Jill B. Harland[b], Amy L. Speelman[b,c,2], Nicolai Lehnert[b], and Stephen W. Ragsdale[a,3]

[a]Department of Biological Chemistry, University of Michigan, Ann Arbor, MI 48109; [b]Department of Chemistry, University of Michigan, Ann Arbor, MI 48109; and [c]Department of Biophysics, University of Michigan, Ann Arbor, MI 48109

Edited by John T. Groves, Princeton University, Princeton, NJ, and approved November 19, 2020 (received for review August 6, 2020)

Rev-Erbβ is a nuclear receptor that couples circadian rhythm, metabolism, and inflammation. Heme binding to the protein modulates its function as a repressor, its stability, its ability to bind other proteins, and its activity in gas sensing. Rev-Erbβ binds Fe^{3+}-heme more tightly than Fe^{2+}-heme, suggesting its activities may be regulated by the heme redox state. Yet, this critical role of heme redox chemistry in defining the protein's resting state and function is unknown. We demonstrate by electrochemical and whole-cell electron paramagnetic resonance experiments that Rev-Erbβ exists in the Fe^{3+} form within the cell allowing the protein to be heme replete even at low concentrations of labile heme in the nucleus. However, being in the Fe^{3+} redox state contradicts Rev-Erb's known function as a gas sensor, which dogma asserts must be Fe^{2+}. This paper explains why the resting Fe^{3+} state is congruent both with heme binding and cellular gas sensing. We show that the binding of CO/NO elicits a striking increase in the redox potential of the Fe^{3+}/Fe^{2+} couple, characteristic of an EC mechanism in which the unfavorable *E*lectrochemical reduction of heme is coupled to the highly favorable *C*hemical reaction of gas binding, making the reduction spontaneous. Thus, Fe^{3+}-Rev-Erbβ remains heme-loaded, crucial for its repressor activity, and undergoes reduction when diatomic gases are present. This work has broad implications for proteins in which ligand-triggered redox changes cause conformational changes influencing its function or interprotein interactions (e.g., between NCoR1 and Rev-Erbβ). This study opens up the possibility of CO/NO-mediated regulation of the circadian rhythm through redox changes in Rev-Erbβ.

heme | Rev-Erb | electro-chemical coupling | redox

Rev-Erbα and -β belong to the nuclear receptor superfamily. They are indispensable components of the circadian rhythm and regulate the expression of genes involved in lipid and glucose metabolism and inflammatory responses (1–9). Rev-Erbs are also implicated in influencing cognitive and neuronal functions (10–12). Nuclear receptors have a characteristic N-terminal region containing a ligand-independent activation domain, Activation Function 1 (AF-1). The AF-1 is followed by a DNA-binding C domain linked to a ligand-binding domain (LBD) via a flexible linker (13). Heme binding to the Rev-Erbβ LBD promotes proteasomal protein degradation, facilitates its interaction with corepressors, and enhances its transcriptional repression activity (8, 14–16).

In Rev-Erbβ-LBD, a Cys-Pro–heme regulatory motif affords the Cys as an axial ligand to Fe^{3+}-heme while a second axial ligation is provided by a distal Histidine (His) residue (Fig. 1*A*) (17, 18). Besides adopting a His/Cys-ligated six-coordinate low-spin (LS) Fe^{3+} state, Rev-Erbβ can undergo a thiol–disulfide redox switch in which the coordinating Cys384 forms a disulfide bond with Cys374 giving rise to a His/neutral residue-ligated Fe^{3+}-heme state (17, 19). A metal-based redox switch equilibrates Rev-Erbβ between the Fe^{3+} and Fe^{2+} states (17–19).

The poise between both thiol–disulfide and the $Fe^{3+/2+}$-heme groups of Rev-Erbβ are important in determining the heme occupancy of the protein in cellulo given that the labile heme pools in the nucleus are in low nanomolar concentrations (~<2.5 nM) (20). Here, we focus on the $Fe^{3+/2+}$ redox couple and how this redox poise contributes to Rev-Erb's ability to be a gas sensor. The heme-binding constants for the different redox states of Rev-Erbβ range over 200-fold, from the Fe^{3+}/thiolate with K_d ~0.1 nM to Fe^{2+} with K_d ~22 nM (15). These K_d values indicate that Rev-Erb would lose a significant amount of heme if it is reduced to the ferrous form, and thus a role as a gas sensor seems incongruent because the Fe^{2+}-heme is known to bind gases. Yet several studies indicate that both Rev-Erbβ and its *Drosophila* analog, E75, are involved in sensing diatomic gases (18, 21, 22).

Here, we demonstrate that Rev-Erbβ contains Fe^{3+}-heme yet still functions as a gas sensor by coupling heme reduction to the binding of CO and NO. Our work explains how and why ferric hemoproteins like Rev-Erbβ are ideal gas sensors.

Results

Rev-Erbβ Predominantly Exists in the Ferric Form in Cells. Responsiveness of nuclear receptors to the redox status of the cell is important in matching homeostasis to the changing metabolic conditions (13). The thiol–disulfide and Fe^{3+}/Fe^{2+}-heme redox switches in Rev-Erbβ allow it to adopt variable heme-coordination spheres and heme affinities (17, 19). This redox switch dictates the protein's heme occupancy under limiting concentrations of cellular labile heme, with Fe^{3+}- and Fe^{2+}-heme exhibiting K_d values of 0.1 and 22 nM, respectively (15, 20). We therefore performed spectroelectrochemical and electron paramagnetic resonance (EPR) experiments to determine the cellular resting redox state of Rev-Erbβ.

Significance

Rev-Erbβ is a heme-responsive transcription factor. Yet, the critical role of heme redox chemistry in regulating the protein's heme occupancy and function as a repressor and gas sensor remains elusive. We show that the heme in Rev-Erbβ exists in the Fe^{3+}-state to be replete under the limiting labile heme pool in cellulo. However, binding and sensing gases require Fe^{2+}-heme. We show that signaling gases can drive Fe^{3+}-heme reduction by electrochemically coupling heme reduction to the tight binding of CO/NO to Fe^{2+}-heme. Our work describes a mechanism to explain how and why Fe^{3+}-hemoproteins like Rev-Erbβ are ideal for in cellulo gas signaling.

Author contributions: A.S., E.L.C., N.L., and S.W.R. designed research; A.S., E.L.C., J.B.H., and A.L.S. performed research; A.S., E.L.C., J.B.H., A.L.S., N.L., and S.W.R. analyzed data; and A.S. and S.W.R. wrote the paper.

The authors declare no competing interest.

This article is a PNAS Direct Submission.

[1]Present address: BioMarin Pharmaceutical Inc., Novato, CA 94949.

[2]Present address: Pacific Northwest National Laboratory, Richland, WA 99354.

[3]To whom correspondence may be addressed. Email: sragsdal@umich.edu.

This article contains supporting information online at https://www.pnas.org/lookup/suppl/doi:10.1073/pnas.2016717118/-/DCSupplemental.

Published January 12, 2021.

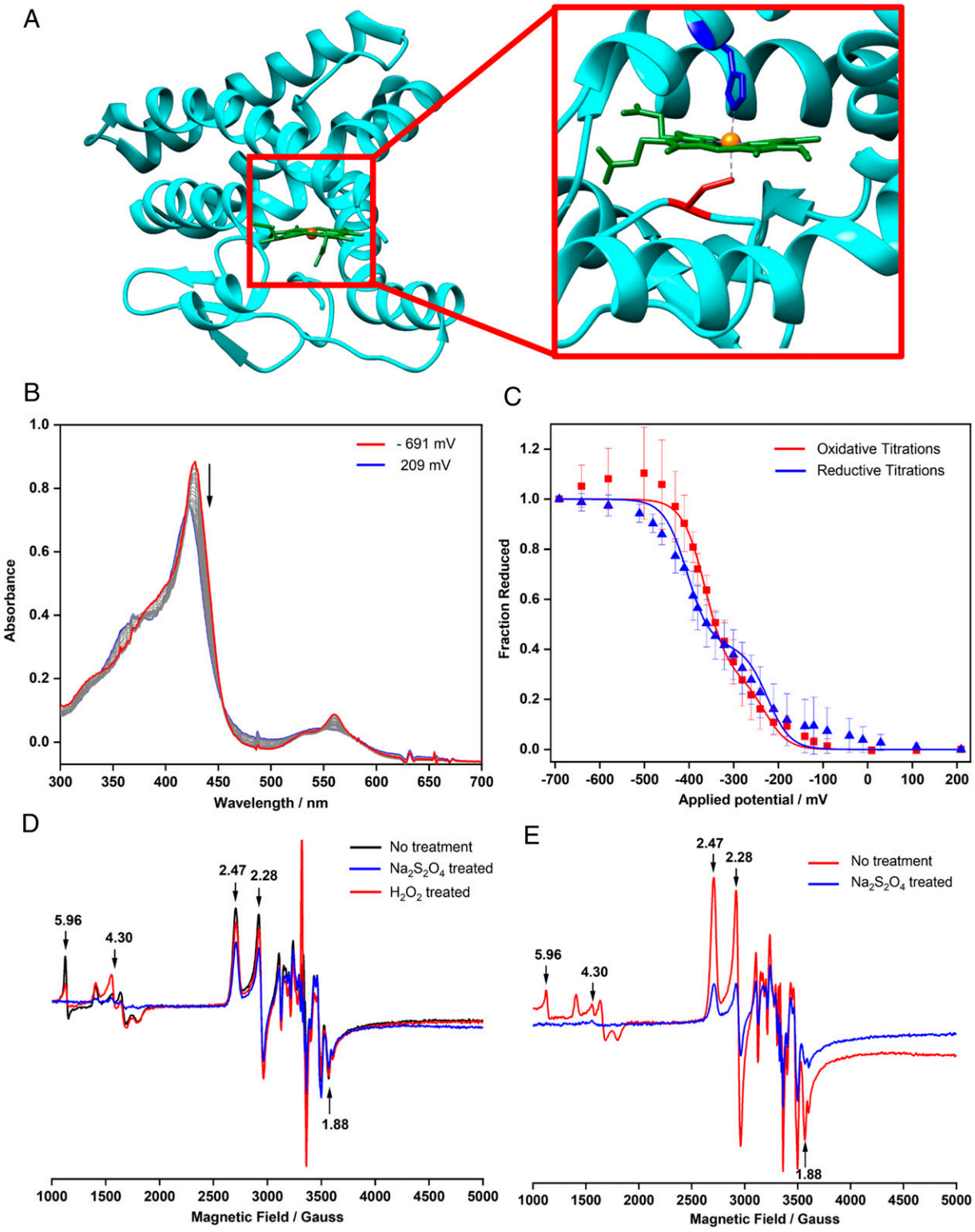

Fig. 1. Rev-Erbβ LBD exists in Fe^{3+}, not Fe^{2+}, form in cellulo. (*A*) Crystal structure of Rev-Erbβ LBD complexed with Fe^{3+}-heme (3CQV), ligand-binding pocket depicting the Fe^{3+}-heme coordinated by Cys (red) and His (blue). (*B*) Spectral changes observed during potentiometric titration of Rev-Erbβ LBD (82 μM). (*C*) Fractional Fe^{2+}-protein (calculated from relative absorption at 559 nm) versus applied potential and theoretical Nernst curves for a one-electron redox reaction. Individual data points are presented as mean ± SD. The redox titrations of the LBD are based on intensity changes in the α bands and include three and five datasets with Soret maxima at 422 nm and 427 nm, respectively. (*D*) EPR spectra of *E. coli* cells overexpressing Rev-Erbβ LBD without any treatment and after incubation with dithionite (20 mM) and H_2O_2 (20 mM) for 3 min. (*E*) EPR spectra of *E. coli* cells overexpressing Rev-Erbβ LBD without any treatment and with a pinch of solid dithionite for 5 min. The g-values for the rhombic feature of the LBD iron (2.47, 2.28, and 1.88), the adventitious iron (4.3), and the HS iron (5.96) are depicted in the EPR spectra. EPR conditions were as follows: temperature, 11 °K; microwave power, 208 μW; microwave frequencies for *D*, 9.3851 (black), 9.3881 (blue), and 9.3902 (red) GHz; for *E*, 9.3840 (red) and 9.3873 (blue) GHz; modulation frequency, 100 kHz; modulation amplitude, 7 G; two scans; and 327.68 ms time constant.

Table 1. Redox properties of Rev-Erbβ LBD

	Reductive titration	Oxidative titration
Amplitude of low redox potential population	0.41 ± 0.03	0.29 ± 0.04
Low redox potential (mV)	−224.9 ± 9.8	−229.4 ± 14.7
Amplitude of high redox potential population	0.59 ± 0.03	0.71 ± 0.04
Low redox potential (mV)	−405.0 ± 6.7	−363.8 ± 5.7

Comparison of the midpoint potentials of the reductive and oxidative titrations. Data from Fig. 1C was fit using Eq. **1**.

By poising the protein solution at increasingly positive potentials (oxidative titrations) from −691 to 209 mV, the λ_{max} of the Soret band shifted from 427 (Fe^{2+} protein) to 422 (Fe^{3+}) nm (Fig. 1 *B* and *C*). The α bands decreased in intensity and shifted from 560 to 570 nm, with the difference spectra showing a maximum absorption decrease at 466 nm and a concomitant increase at 560 nm (*SI Appendix*, Fig. S1*A*). In some of the titrations, the λ_{max} of the Soret band for the Fe^{2+} protein was observed at 422 nm as opposed to the expected 427 nm (*SI Appendix*, Fig. S1*B*).* The titrations were reversible with the Nernst fits indicating the existence of two populations of the protein with fairly low redox potentials. The calculated midpoint potentials for reductive titrations were −224.9 mV and −405.0 mV and for the oxidative titrations were −229.4 mV and −363.8 mV (Fig. 1*C* and Table 1). Given that the redox potential within the nucleus is ∼−280 mV, it appears that the protein equilibrates between the Fe^{3+} and Fe^{2+} states with the majority of heme in the Fe^{3+} state (23).

Previously reported magnetic circular dichroism (MCD) and Resonance Raman studies of the Rev-Erbβ LBD indicated the presence of two Fe^{2+}-heme populations (17). Our MCD experiments with longer LBD constructs (including residues 275 through 357) than previously reported also show the presence of a mixture of five-coordinate high-spin (HS) and six-coordinate (6c) LS Fe^{2+}-heme populations. The two Fe^{2+} populations were characterized by the temperature-dependent C-term and the temperature-independent A-term respectively (*SI Appendix*, Fig. S2*A*). These MCD data agree with the conclusion of the electrochemical titrations that Rev-Erbβ contains two Fe^{2+}-heme populations. Our MCD experiments with the full-length and the LBD protein display identical spectral features (*SI Appendix*, Fig. S2*B*) demonstrating that the LBD retains the heme-coordination sphere of the full-length protein and hence serves as a prototype for the full-length protein (17). Furthermore, similar MCD spectra were obtained for the protein bound to NCoR1 and DNA (*SI Appendix*, Fig. S2*B*), indicating that the different domains of Rev-Erbβ behave as modules rather than as tightly coupled units (13).

Heme binding is key to regulating Rev-Erb's downstream activities. Given the different affinities of Rev-Erbβ for Fe^{3+}-(K_d = 0.1 nM) versus Fe^{2+}-heme (K_d = 22 nM) (15), heme redox chemistry can define its heme occupancy, resting state, and activity. Thus, at the reported value of the labile heme pool in the nucleus of <2.5 nM (20), only the Fe^{3+} form of this nuclear receptor would be heme replete. Our experiments suggest that Rev-Erbβ evolved its tight-binding Fe^{3+}-heme–binding site to accommodate to this stringent environment of heme scarcity. Correspondingly, the low-redox potential of its Fe^{3+}/Fe^{2+} couple poises the heme mostly in the Fe^{3+} state. Only when nuclear heme concentrations increase significantly (e.g., under conditions of heme overload [>100 nM]), the redox poise would not determine heme-occupancy and Rev-Erbβ would contain a mixture of Fe^{3+}- and Fe^{2+}-heme. Under these conditions, given the low redox potential of Rev-Erbβ, the protein would be mostly Fe^{3+}-heme bound and the other population would be Fe^{2+}-heme bound but not the heme unbound, aka the apo, state. However, the heme concentrations are very tightly regulated in the cellular milieu by a plethora of systems including heme chaperones and transporters, up-regulation of heme degradation by the heme oxygenase system, and down-regulation of heme synthesis (24–26).

Whole-cell EPR spectroscopy of *Escherichia coli* cells overexpressing the LBD validated the spectroelectrochemical results indicating that Rev-Erbβ exists in the Fe^{3+} form under normoxic cellular redox conditions. It has not yet been possible to obtain high enough concentrations of Rev-Erbβ to perform these experiments in human cells. We used *E. coli* as a model system to study the redox status of Rev-Erbβ in a cellular environment mimicking the redox poise of the human cell nucleus, which appears to be similar to that of the cytosol (19, 27–32). *E. coli* cells overexpressing the protein showed a rhombic EPR spectrum, a feature that was not seen for control cells containing the empty plasmid, lacking the Rev-Erbβ gene. Moreover, the rhombic EPR spectrum exhibited g-values (g = 2.48, 2.27, and 1.88) (Fig. 1 *D* and *E*) that are identical to those of the purified protein, consistent with His/Cys coordinated Fe^{3+}-heme, as seen in the crystal structure (Fig. 1*A*).

We reasoned that if cellular Rev-Erbβ contained significant amounts of Fe^{2+}-heme, treatment with an oxidant would enhance the EPR signal. However, addition of H_2O_2 increased the signal intensity of extraneous cellular heme (g = 4.30) but not that of the LBD Fe^{3+}-heme. Instead, a modest (∼15%) signal loss was observed. On the other hand, treatment with the reductant dithionite (20 mM) caused a 36% decrease in EPR signal intensity from the LBD (Fig. 1*C*) as the Fe^{3+} form of the LBD was reduced to the EPR-silent Fe^{2+} form. A more pronounced (∼73%) signal reduction occurred upon solid dithionite treatment for 5 min (Fig. 1*D*). As expected, dithionite treatment also decreased the EPR signal intensities at g = 4.30 and 5.96. Thus, our combined spectroscopic and electrochemical studies demonstrate that within the cell, Rev-Erbβ primarily exists as 6c His/Cys ligated with Fe^{3+}-heme and that binding to neither DNA nor corepressor alters this property as was apparent from the MCD experiments.

Ferric Rev-Erbβ as CO Sensor. We next focused on the apparent conundrum of how this Fe^{3+} protein could function as a gas sensor when it is recognized that only Fe^{2+}-heme can bind CO and NO with high affinity (18, 21, 22). Recognizing that the iron coordination sphere has a significant impact on its redox potential (E^0), we reasoned that CO binding to Rev-Erbβ could increase the apparent redox potential of the $Fe^{3+/2+}$ redox couple (33). CO introduction into the electrochemical setup containing low-potential dyes resulted in a color change of the solution from orange-red (typical of the Fe^{3+} protein) to pink. The Soret absorption maximum shifted to 421 nm and the Q-bands exhibited maxima at 539 nm and 570 nm, characteristic of Fe^{2+}-CO–bound protein (Fig. 2*A*). This reaction is apparently

*However, the dithionite-reduced protein always shifted to 427 nm (*SI Appendix*, Fig. S9). EPR experiments ensured the integrity of the ferric protein (*SI Appendix*, Fig. S8). Thus, we tentatively attribute the altered Soret absorption to an interaction between Rev-Erb and the redox mediators. Changes resulting from the datasets with no shift in the λ_{max} of the Soret band for the ferrous protein are depicted in *SI Appendix*, Fig. S1*B*.

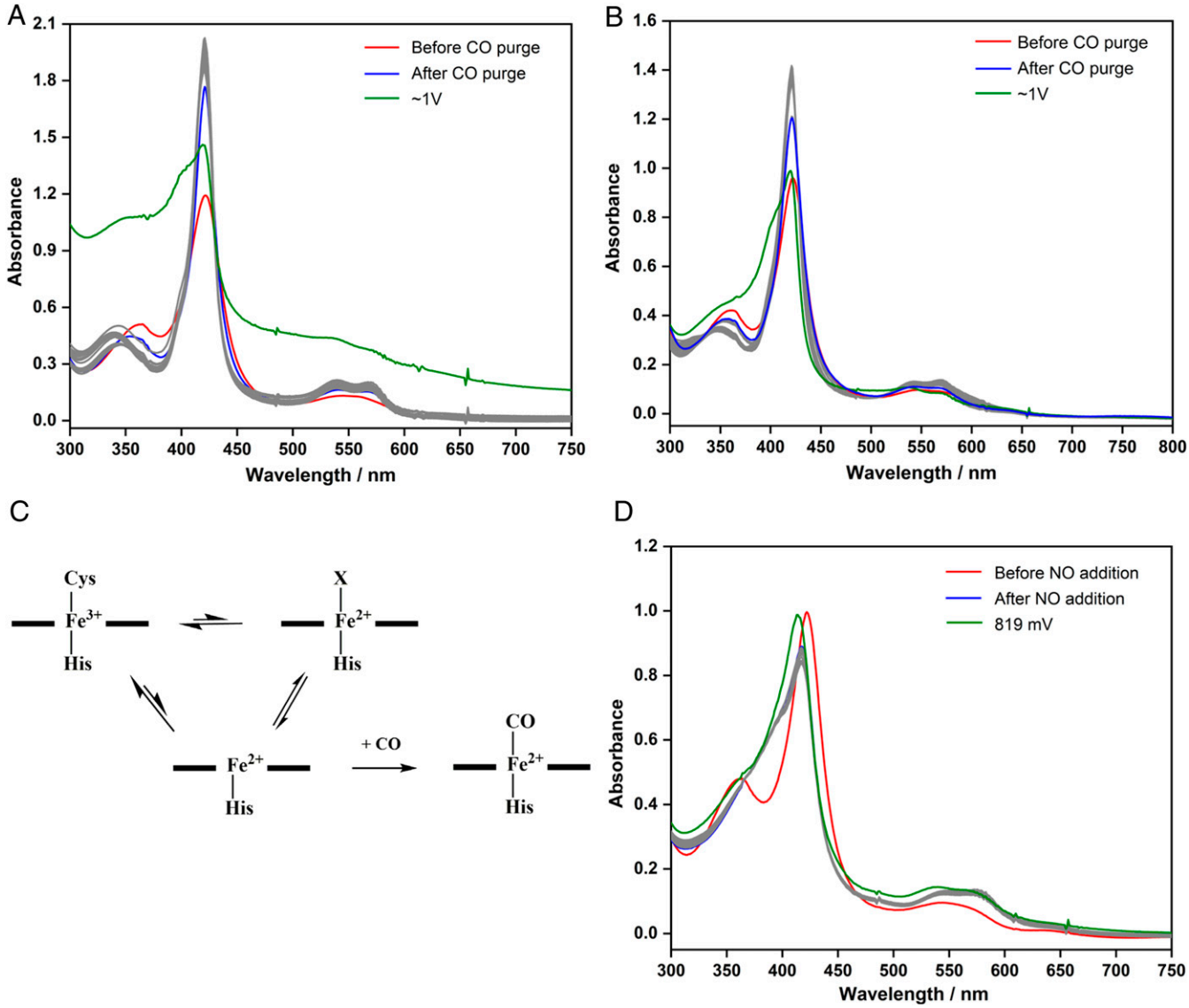

Fig. 2. Redox properties of Rev-Erbβ LBD in presence of CO and NO. Spectral changes observed during potentiometric titration of Rev-Erbβ LBD , with low-potential redox mediators under CO atmosphere. [LBD] = 118.5 μM (*A*) and with high- and low-potential redox mediators under CO atmosphere. [LBD] = 95.5 μM (*B*). Gray traces represent absorption at potentials from 159 to 959 mV in *A* and −11 to 959 mV in *B*. (*C*) proposed scheme of CO-mediated Fe^{3+}-LBD reduction. (*D*) Potentiometric titration of LBD with high- and low-potential redox mediators in presence of NO. Gray traces represent absorption at potentials from 189 to 789 mV. LBD = 99.1 μM.

irreversible because oxidative titrations of the CO-bound protein at potentials as high as +959 mV did not elicit any noticeable reoxidation (Fig. 2*A*). We stopped the experiment at a potential of 989 mV because the protein began to precipitate. Even when both low- and high-potential redox mediators were included in the experiment (Fig. 2*B*), no change in the Fe^{2+}-CO spectrum was observed. These results demonstrate that the binding of CO increases the apparent redox potential of the $Fe^{3+/2+}$ couple of the LBD heme by over 1.2 V.

The autoreduction of heme proteins driven by a water–gas shift reaction in the absence of a reductant has been observed in cytochrome c oxidase, hemoglobin, and myoglobin (34). To test this possibility, we monitored conversion of ^{13}CO to $^{13}CO_2$ by the LBD protein using gas chromatography–mass spectrometry and quantified the $^{13}CO_2$ production in the headspace with respect to $^{12}CO_2$ using CODH as a positive control (35). The $^{13}CO_2/^{12}CO_2$ ratio for Rev-Erbβ was similar to that of control experiments lacking the LBD and was significantly lower than the CODH control (*SI Appendix*, Fig. S3). Thus, CO oxidation does not drive heme reduction in Rev-Erbβ.

Formation of Rev-Erbβ Fe^{2+}-CO was also not driven by the intramolecular electron transfer from Cys thiolates to Fe^{3+}-heme resulting in protein dimerization under CO atmosphere, as observed with the Cys variants of myoglobin (36). Our sodium dodecyl sulfate polyacrylamide gel electrophoresis (SDS-PAGE) analysis showed no increase in the LBD-dimer band intensity in the presence of CO (*SI Appendix*, Fig. S4 *A* and *B*). Furthermore, unlike the mechanism of heme reduction delineated by Hirota et al. (36), which solely relies on protein thiolates as the electron source, the Fe^{3+} to Fe^{2+}-CO transition in Rev-Erbβ requires low-potential redox mediators (*SI Appendix*, Fig. S4*C*).

The gargantuan >1.2 V increase in midpoint potential of the $Fe^{3+/2+}$ couple when CO binds to the LBD evokes an EC mechanism in which electrochemistry is coupled to a chemical

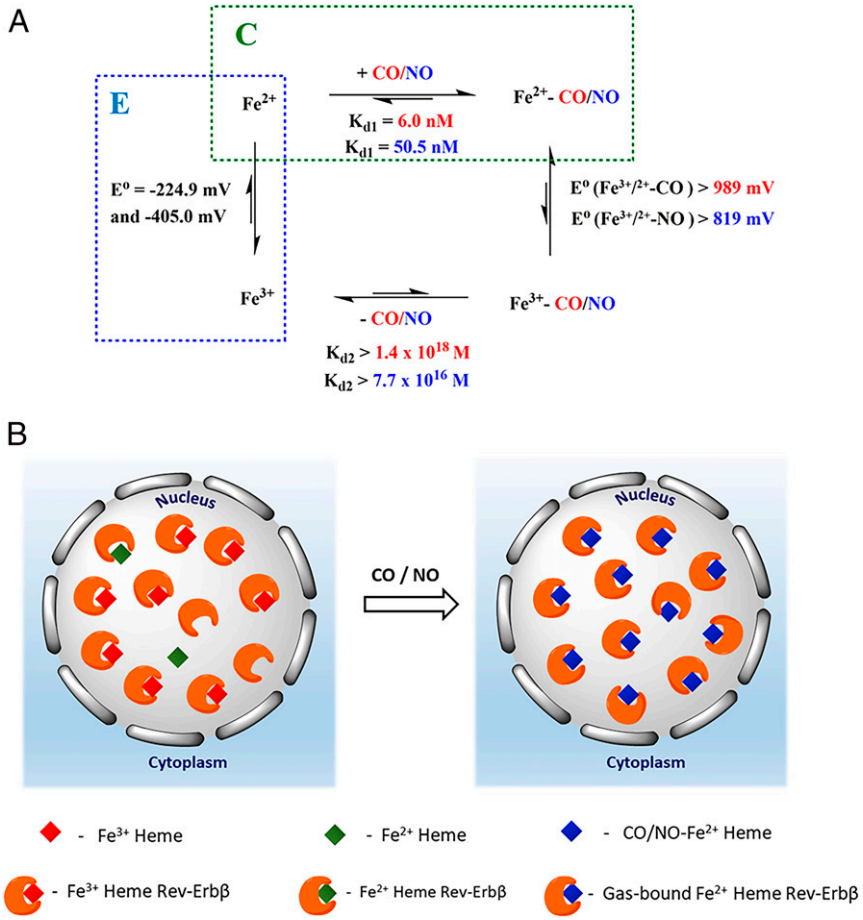

Fig. 3. Gas-driven reduction of Fe^{3+} Rev-Erbβ by the EC mechanism allowing Fe^{3+}-heme to function as a gas sensor. (*A*) Thermodynamic box depicting redox potentials and gas-binding constants of different redox and gas-bound states of Rev-Erbβ LBD. Red and blue indicate thermodynamic parameters for CO and NO, respectively. E^0 and E^0 ($Fe^{3+/2+}$-CO/NO) represent the redox potentials of the Fe^{3+}/Fe^{2+} couple in absence and presence of CO/NO, respectively. K_{d1} and K_{d2} represent the binding constants of the Fe^{2+} and Fe^{3+} protein to CO and NO, respectively. K_{d1} for CO = 6 nM (14). Coupling of electron transfer with chemical reaction is depicted by the blue and green boxes; (*B*) Our experiments suggest that Rev-Erbβ predominantly exists in a Fe^{3+}-heme–bound state in cells. Under limiting concentrations of intracellular labile heme pools, Fe^{3+}, not Fe^{2+}, Rev-Erbβ remains in the heme-replete state. Signaling gases such as CO and NO exert a thermodynamic pull that allows the protein to be in the reduced gas-bound form. This intriguing redox chemistry allows the protein to shuffle between Fe^{3+} and Fe^{2+} heme states thereby not limiting Rev-Erb's function as a gas sensor even when the protein primarily exists in the oxidized form.

reaction (Fig. 3). At ~ −280 mV, redox poise within the nucleus, Rev-Erbβ would exist mainly in the Fe^{3+} form. However, the strong interaction of the residual Fe^{2+}-heme with CO (K_d = 6 nM) (14) exerts a driving force to push the thermodynamically unfavorable heme reduction to yield ~100% reduced protein (Fig. 2*C*).

We quantified the populations of the oxidized and reduced proteins under different conditions and constructed a thermodynamic box (Fig. 3*A*) to derive the unknown thermodynamic parameters. Our redox titrations revealed two populations with E° (standard redox potential) values of −0.225 V and −0.405 V and relative amplitudes of 0.4136 and 0.5864, respectively (Table 1 and Fig. 3*A*, box E). Taking into account the amplitudes of each population, the ratio of the reduced (37.5%) to oxidized (62.5%) states at a potential (E) of −280 mV (the redox potential within the nucleus) (23) was calculated based on the Nernst equation to be 1.7 (*Materials and Methods*).

However, this ratio of the oxidized and reduced protein drastically changes in the presence of CO (Fig. 3*A*, boxes E and C). Our redox titrations indicate the E° for the Fe^{3+}-CO/Fe^{2+}-CO equilibrium to be higher than 989 mV. The ratio of the reduced to oxidized protein in the presence of CO at a potential of −280 mV for an E^0 of 989 mV is greater than 10^{21} (*Materials and Methods*). Thus, the heme in Rev-Erbβ is fully reduced when the electrochemistry is performed under a CO atmosphere.

Using these data, the dissociation constant (K_{d2}) for CO from the Fe^{3+}-CO complex (Eq. **7**) is calculated to be greater than 1.39×10^{18} M. Thus, the high stability of Fe^{2+}-CO (K_d = 6 nM) excludes formation of Fe^{3+}-CO. To achieve even a 50% conversion of Fe^{3+} protein to the Fe^{3+}-CO form would require CO concentrations close to 10^{18} M. Therefore, regeneration of the resting Fe^{3+} state of Rev-Erbβ from the Fe^{2+}-CO state would only occur when the cellular CO concentration drops below the 6 nM K_d value, generating the Fe^{2+} state, which would be in unfavorable $Fe^{3+/2+}$ redox equilibrium at the cellular redox poise.

Ferric Rev-Erbβ as NO Sensor. When Rev-Erbβ is treated with the gaseous signaling molecule NO, its transcriptional repression activity markedly decreases, suggesting it to be an NO sensor (18). As with CO, NO addition to the Fe^{3+} protein resulted in the formation of Fe^{2+}-NO, with a blue shift in the Soret band from 422 to 417 nm (Fig. 2*D*). The EPR spectrum of the NO adduct showed a multiline spectrum typical of a NO- and His-bound heme in which the unpaired spin on NO couples to the coordinating His nitrogen trans to the bound-NO (Fig. 4*B*) (17). Potentiometric oxidation in the presence of NO elicited no redox

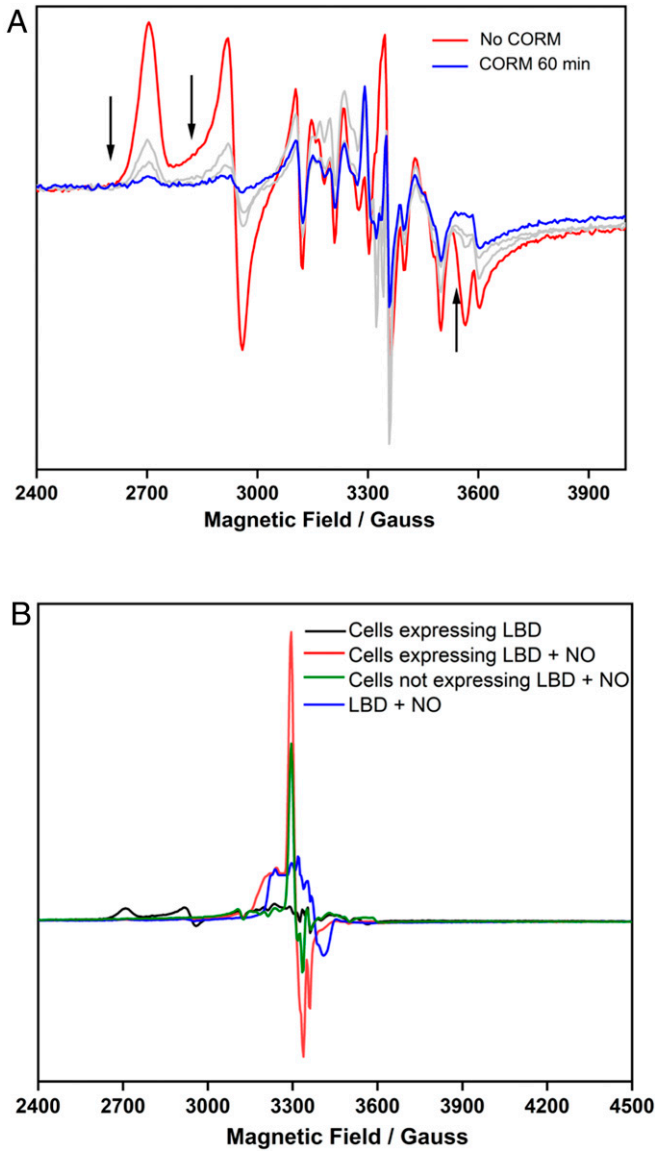

Fig. 4. Effect of CO and NO on the redox state of Rev-Erbβ in cellulo. (*A*) EPR spectra of *E. coli* cells overexpressing LBD with and without 20 mM CORM-A1 treatment for variable times (20, 40, and 60 min). Full EPR spectra are shown in *SI Appendix*, Fig. S7*A*. EPR conditions were as follows: temperature, 11 °K; microwave power, 20 μW; microwave frequencies, 9.3803, 9.3797, 9.3808, and 9.3795 GHz; modulation frequency, 100 kHz; modulation amplitude, 7 G; two scans; and 327.68 ms time constant. (*B*) EPR spectra of 1) *E. coli* cells overexpressing LBD with and without Proline NONOate treatment (10 mM, 6 min), 2) *E. coli* cells containing empty vector pMCSG9 after Proline NONOate treatment (10 mM, 6 min), and 3) Rev-Erbβ after Proline NONOate addition. EPR conditions were as follows: temperature, 11 °K; microwave power, 20 μW; microwave frequency, 9.3831 and 9.3823 GHz for 1, 9.3840 GHz for 2, and 9.3849 GHz for 3; modulation frequency, 100 kHz; modulation amplitude, 3 G; four scans; and 327.68 ms time constant.

transition at up to 789 mV (Fig. 2*D*). The protein began to precipitate at a potential of 820 mV, similar to the Fe^{2+}-CO titration, indicating a much higher stability of the Fe^{2+}-NO complex than the Fe^{3+}-NO complex ($>10^{24}$) (Fig. 3). This high stability is imparted by the strong affinity (K_d = 50.5 nM) of the Fe^{2+}-LBD for NO (*SI Appendix*, Fig. S6), which drives the thermodynamically unfavorable heme reduction. NO can reduce Rev-Erbβ in the absence of redox mediators (*SI Appendix*, Fig. S5*A*), implying that NO can possibly serve as a source of electrons in cellulo to facilitate the reduction of Rev-Erbβ. Reductive nitrosylation can proceed either by inner- or outer-sphere electron transfer from NO to the metal center followed by the attack of a nucleophile. The nucleophile can be an OH^- or a ligand coordinating or in vicinity to the heme pocket such as thiolate (37). The net result is the formation of HNO_2 or a nitrosothiol and Fe^{2+}-heme that can further react with a second equivalent of NO to yield Fe^{2+}-NO heme. We do not observe formation of nitrite, suggesting a Cys-S-NO–related heme reduction. Regardless, the stability conferred by NO to trap Rev-Erbβ in the reduced state may as well be a cellular signaling mechanism for sensing NO, in turn regulating the biochemical and cellular activities of Rev-Erbβ.

Rev-Erbβ Fe^{3+}-Heme: A Gas Sensor in Cells. To complement the in vitro experiments, we used whole-cell EPR to determine if CO and NO convert Fe^{3+}-heme to the EPR-silent Fe^{2+}-CO or Fe^{2+}-NO state in cellulo. When cells were treated with the CO-releasing molecule CORM-A1, the Fe^{3+}-heme EPR signal decreased by 70% within 20 min (Fig. 4*A* and *SI Appendix*, Fig. S7*C*) and nearly disappeared (93.0%) after 60 min of CORM treatment. CORM treatment also decreased the six-line spectrum cellular Mn^{2+} and high-spin heme and modestly reduced the signal of extraneous nonheme iron (*SI Appendix*, Fig. S7 *D* and *E*).

Addition of proline NONOate, which generates NO, to LBD-overexpressing *E. coli* cells elicits a response similar that of CO. NO treatment results in a concentration-dependent loss of the Rev-Erb Fe^{3+}-heme signal (*SI Appendix*, Fig. S5*B*). This reduction is accompanied by gain of a signal at g = 2.06 and 2.03 (Fig. 4*B*). The signal increase at g = 2.03 is also observed for control cells containing the empty vector (*SI Appendix*, Fig. S5*C*) and can be attributed to the reaction of NO with iron–sulfur clusters yielding dinitrosyl iron complexes (38). The signal build-up at g = 2.06 is also observed upon the treatment of the LBD with NO (Fig. 4*B*), confirming nitrosylation of the Fe^{3+}-heme of Rev-Erbβ in cellulo.

Discussion

Our in vitro and whole-cell experiments demonstrate that the low-$Fe^{3+/2+}$-heme redox potential of Rev-Erbβ dictates that it rests in the Fe^{3+} state in cells. Given the 220-fold higher affinity of the LBD for Fe^{3+}- versus Fe^{2+}-heme, having a low-$Fe^{3+/2+}$ redox potential allows Rev-Erb to be heme replete at the low-nM concentrations of labile heme in the nucleus until the cell is exposed to gaseous-signaling modulators such as CO and NO when it gets reduced (Fig. 3*B*). This phenomenon is attributed to the high stability of the gas-bound Fe^{2+} state over the Fe^{3+}-state. Rev-Erbβ takes advantage of this high stability by linking heme reduction (electrochemistry) to gas binding (chemistry) via an EC mechanism. Accordingly, an increase in the apparent redox potential of the Fe^{3+}/Fe^{2+} couple in presence of the signaling gases is observed. Recycling Rev-Erb to its resting Fe^{3+} state would occur when the cellular concentrations of CO or NO drop below the K_d-value. Our work establishes how Fe^{3+}-Rev-Erbβ functions as a gas sensor when signaling gases (CO and NO) selectively bind the Fe^{2+} state of the metallocofactor (16). Our findings explain why NO is able to alleviate transcriptional repression by Rev-Erbβ, which rests in the Fe^{3+} state, in mammalian cells (18).

The EC mechanism of ligand-driven redox coupling invoked here for the modulation of a transcriptional regulator is important in fundamental chemical and biological processes where redox changes are accompanied by ligand, substrate, and proton binding and/or conformational changes (39–41). Not only signaling gases but various substrates or ligands can be interfaced with the $Fe^{3+/2+}$ redox couple. A well-studied example is Cytochrome P450, which, because of its low $Fe^{3+/2+}$ potential, is predominantly in the Fe^{3+} state within the cell (42). Substrate

binding increases this potential, promoting reduction to the Fe^{2+} state, which binds O_2 and initiates the formation of reactive iron-oxo catalytic intermediates involved in substrate oxidation. Perhaps for many of these systems, having a low-redox potential is important for keeping them in the metal-replete oxidized state so that they only become active when their ligands appear in solution.

Our findings offer a fundamental explanation as to how and why chemical gating of electron transfer in hemoproteins like Rev-Erbβ allows them to exist in the oxidized form but still function as a gas sensor (43–46). Thus, Rev-Erbβ (and potentially other heme-based signaling proteins) seem ideally poised to function as both heme- and gas-regulated nuclear receptors to control myriad processes like regulation of the circadian rhythm, glucose and lipid metabolism, and inflammatory responses.

Further, in cellulo studies are required to survey the resting states of other cellular redox-active metalloproteins and to correlate these results with the redox poise of their cellular microenvironment, reduction potential of their metal cofactor, and ligand-binding constants (K_d values). It's also important to examine the structural effects of these redox- and/or ligand-binding reactions which are often accompanied by conformational changes that alter a protein's interactome and functions.

Moreover, CO and NO are increasingly recognized as important regulators of the circadian rhythm. However, the molecular mechanisms underlying the same remain elusive. We anticipate that this work will pave the way for investigating how CO/NO can be integrated into the circadian rhythm framework due to their ability to cause redox reactions in metalloproteins like Rev-Erbβ.

Materials and Methods

Unless otherwise mentioned, all chemicals were of analytical grade, obtained from commercial sources, and used without further purification. All experiments were performed in 0.5× TNG (25 mM Tris HCl, 150 mM NaCl, and 5% glycerol) pH 8.0 buffer unless otherwise mentioned. Experiments involving the use of Proline NONOate and CORM-A1 were performed in 0.5× TNG pH 7.4 buffer. All absorption measurements were carried out on an Agilent Cary 8454 ultraviolet (UV)-visible (vis) spectrophotometer inside the anaerobic chamber with less than 0.3 ppm dioxygen except for Bradford assays and heme concentration measurements, which were performed aerobically on a Shimadzu UV-2600 spectrophotometer. The Rev-DR2 DNA sequence was obtained from Integrated DNA Technologies (Coralville, IA).

Protein Expression and Purification. The Rev-Erbβ LBD encompassing residues 370 through 579 was expressed as described previously (15). Briefly, the Rev-Erbβ LBD is expressed as a translational fusion between maltose binding protein (MBP) and the LBD protein separated by an internal tobacco etch virus (TEV) protease cleavage site. The fusion protein was expressed in *E. coli* BL21(DE3) cells grown at 37 °C in Terrific Broth supplemented with 0.4% glycerol and 200 $\mu g/mL^{-1}$ ampicillin. Protein expression was induced with 0.5 mM isopropyl β-D-1-thiogalactopyranoside. The cell pellet obtained by centrifugation was suspended in TNG buffer (50 mM Tris·HCl, pH 8.0, 300 mM NaCl, and 10% glycerol) containing 1 mM dithiothreitol, 6 mM benzamidine, 1 mM EDTA, 0.5 mM phenylmethanesulfonyl fluoride, and 1× protease inhibitor mixture (Roche Applied Science) on ice and lysed by sonication. The cell-free extract obtained post centrifugation was applied to an amylose column (New England Biolabs) equilibrated in TNG with 1 mM DTT at 4 °C. After washing the column with the TNG buffer, the pure fusion protein was eluted with TNG containing 20 mM maltose. MBP tag was removed by TEV protease treatment. Removal of the cleaved MBP tag was achieved by passing the protein solution through a hydroxyapatite column. The protein was eluted using a buffer containing 20 mM sodium phosphate, 200 mM NaCl, and pH 7.2. The eluted protein was concentrated and buffer exchanged into 0.5× TNG buffer using an Amicon ultrafiltration device (Millipore) containing a 10-kDa membrane.

The heme content in the protein was determined by the pyridine hemochrome assay (47). The heme content varied from 10 to 20% approximately between different batches.

MCD experiments were performed with slightly longer LBD constructs (residues 247 through 57) of Rev-Erbβ than previously reported. The LBD was expressed and purified as an N-terminal His_6-tagged protein according to the previously reported protocol (19). MBP-NCoR1 protein containing all three interaction domains and full-length MGC Rev-Erbβ used for MCD studies were purified according to the previously reported protocol (14).

Preparation of Thiol-Reduced Protein. Thiol-reduced protein was prepared in an OMNI-LAB anaerobic chamber (vacuum atmosphere) maintained with N_2 atmosphere containing <0.3 ppm dioxygen. The protein was treated with >10-fold excess of TCEP in aqueous solution (Sigma) and incubated for an hour in the anaerobic chamber at room temperature. The thiol-reduced protein was exchanged into anaerobic 0.5× TNG buffer using Microbiospin 6 columns (Bio-Rad). The protein concentration was determined by the Bradford assay (Thermo Fisher Scientific). To prepare the heme-bound protein, a primary heme stock was prepared by dissolving hemin in 0.1 M NaOH and 10% DMSO. The solution was filtered through 0.2 μm DMSO-safe syringe filters (Pall Corporation) and diluted to ∼1 mM in 0.5× TNG. The concentration of the secondary stock was determined from the absorption at 385 nm ($\varepsilon = 58.44\ mM^{-1} \cdot cm^{-1}$) (48). Because the heme content of the protein varied from 10 to 20% between batches, the thiol-reduced protein and external heme were mixed in the ratio of either 1:0.6 or 1:0.5, respectively, under anaerobic conditions. For all experiments, heme was added at substoichiometric concentration to the protein to avoid any spurious effect from unbound heme. Concentrations of protein reported are that of the heme-bound protein calculated from the Soret peak unless otherwise mentioned.

Redox Titrations. Redox titrations were performed at 25 °C in an anaerobic chamber with < 0.3 ppm O_2. All experiments were performed in 0.5× TNG anaerobic buffer. Two mixtures of mediator dyes (with 1 mM of each dye), low potential dyes (Table 2), and high potential dyes (Table 3) were prepared in 0.5× TNG buffer (pH 7.4 or 8.0) for the redox titrations.[†] Triquat and dimethyl triquat were synthesized according to previously reported protocol (49).

The redox mediator dyes were added to the thiol-reduced protein at molar ratios of 1:10. The redox titrations were carried out in an electrochemical cell (BASI) equipped with three electrodes (Au gauze as working electrode, Pt as auxiliary electrode, and Ag/AgCl as reference electrode) connected to a CV-27 voltammogram (BASI). The applied potential was varied from 0 to −900 mV versus Ag/AgCl. The redox titrations were followed by

Table 2. Low potential dyes used in the redox titrations

Dyes	Potential (mV)*	Ref.
Potassium indigotetrasulfonate	−46	51
Indigo carmine	−125	51
Anthraquinone-1,5-disulfonic acid	−200	52
Anthraquinone-2-sulfonic acid	−225	45
Benzyl viologen	−358	45
Methyl viologen	−440	45
Triquat	−549	53
Dimethyl triquat	−684	53

*All potentials are reported versus the standard hydrogen electrode.

Table 3. High potential dyes used in the redox titrations

Dyes	Potential (mV)*	Ref.
Methylene blue	11	51
Methyl hydroquinone	460	54
Thionine	56	51
N-Acetyl L-tryrosinamide	650	54
Adenine	750	54
Potassium indigotetrasulfonate	−46	51
Indigo carmine	−125	51
Methylene green	123	55
Bindscheder's green[†]	224	51

*All potentials are reported versus the standard hydrogen electrode.

[†]Bindscheder's Green was sparingly soluble in 0.5× TNG buffer and had to be handled anaerobically. Unlike others, the stock concentration of Bindscheder's Green was less than 1 mM.

CHEMISTRY

monitoring the absorption changes of the protein inside the anaerobic chamber. The absorption spectrum reported at each potential was recorded after no further change in absorption was observed and/or the current reached 0 μA. The LBD heme redox potential (E°) was determined from the Nernst-plot of the fraction of protein-reduced versus the applied potential. The data best fit to a one-electron redox reaction with two populations (Eq. **1**), the [red] and [oxd] represent concentrations of reduced and oxidized protein, respectively; $E°_1$ and $E°_2$ represent the redox potential of the two populations; and a and b represent the amplitude of two populations with the constraint a + b = 1. All the redox potentials are reported against the standard hydrogen electrode unless otherwise mentioned. The r^2 values (0.991 and 0.988 for the oxidative and reductive titrations) strongly support the biphasic fits, as shown, as compared to monophasic curves (0.955 and 0.839, respectively). Furthermore, a two-potential model is supported by the MCD data, which reveal two forms of the reduced Fe^{2+}-protein (as described here):

$$\frac{\text{red}}{\text{red}+\text{oxd}} = \frac{\text{a}}{e^{0.0389\times(x-E°_1)}} + \frac{\text{b}}{e^{0.0389\times(x-E°_2)}}. \quad [1]$$

Redox titrations in presence of CO were done by purging the headspace of the electrochemical cell with CO. CO was also purged intermittently to maintain a positive pressure of CO throughout the experiment. Proline NONOate (Cayman Chemicals) was used as the source of NO for redox titrations. Proline NONOate stock solutions were prepared in 10 mM NaOH. The applied potential was varied from 209 to −691 mV for the reductive and oxidative titrations in absence of gases. Redox titrations in presence of CO were carried out in the presence of low-potential dyes and a combination of low- and high-potential dyes with the applied potentials for the two experiments varying from 159 mV to 1 V and from −11 to 989 mV, respectively. Redox titrations in presence of excess NO (~2 mM) were carried out in the presence of both low- and high-potential dyes with the applied potential varying from 189 to 819 mV.

MCD Studies. All MCD experiment samples were prepared in 25 mM Tris, 150 mM NaCl, 50% glycerol (added as a glassing agent), and pH 8.0 buffer. The LBD ferrous protein preparations also had 5 mM dithionite in the solution. The proteins of interest were injected between two quartz plate windows housed in a custom-made MCD sample holder. The samples were frozen in liquid nitrogen to produce glass.

An OXFORD SM4000 cryostat and a JASCO J-815-CD spectrometer were used for the MCD setup. The SM4000 cryostat consisting of a liquid helium-cooled superconducting magnet provided horizontal magnetic fields of 0 to 7 T. The J-815 spectrometer uses a gaseous nitrogen-cooled xenon lamp and a detector system consisting of two interchangeable photomultiplier tubes in the UV-vis and near-infrared spectroscopy range. The samples were loaded into a 1.5 to 300 K variable temperature insert, which offers optical access to the sample via four optical windows made from Suprasil B quartz. The MCD spectra were measured in [θ] = mdeg and manually converted to Δε (M^{-1} cm^{-1} T^{-1}) using the conversion factor

$$\Delta\varepsilon = \frac{\theta}{32980 \times c \times d \times B} \quad [2]$$

where c is the concentration in Molar (M), B is the magnetic field in Tesla (T), and d is the path length in centimeter (cm). The product $c \times d$ can be substituted by $A_{MCD}/\varepsilon_{UV\text{-}vis}$, where A_{MCD} is the absorbance of the sample measured by the CD spectrometer and $\varepsilon_{UV\text{-}vis}$ is the molar extinction coefficient. Complete spectra were recorded at indicated temperatures and magnetic fields.

SDS PAGE Analysis. SDS PAGE analysis to probe protein dimer formation under CO atmosphere was performed on a gradient 4 to 20% SDS gel in the absence of any thiol-reducing agent. Equal concentration and volumes of thiol-reduced LBD protein were incubated at room temperature under N_2 or CO atmosphere for 21 h before running gel electrophoresis and measuring the absorption spectrum of the sample. The gel images were obtained on the ChemiDoc MP Imaging system (Biorad) and the intensity analysis of the bands was done using FijiJ.

GC-MS Studies. $^{13}CO_2$ and $^{12}CO_2$ detection were performed on an Agilent 7980B Gas Chromatograph coupled to 5977B Mass Spectral Detector. The thiol-reduced protein (60 μM) was prepared as described previously. CODH (4.8 μM) was used as a positive control. The samples (600 μL) were prepared and transferred in the anaerobic chamber in vials septum-sealed vials that were then crimp sealed with an aluminum cover (Agilent) and degassed before the introduction of CO. CO was bubbled into the solution for 105 s. A total of 500 μL of the sample was injected and passed through a Carboxen-1010 PLOT Capillary GC column (Sigma, 30 m × 0.32 mm) kept at 25 °C. Helium was used as the carrier gas. The mass spectrometer was used in selected ion monitoring mode for detection of $^{12}CO_2$ and $^{13}CO_2$ at m/z of 44 and 45, respectively. The samples were run for a total time of 10.8 min with data acquisition from 5 to 10.8 min. The retention time for CO_2 was 9.9 min.

The extent of conversion of ^{13}CO to $^{13}CO_2$ was reported as the ratio of the area under the peaks. The percentages of $^{13}CO_2$ with respect to $^{12}CO_2$ represent the average ± SD from three to four acquisitions.

NO Binding Assay. The binding affinity of Fe^{2+}-LBD protein for NO was determined by UV-vis spectrophotometry. The spectrophotometric studies were carried out on an Agilent Cary 8454 UV-vis diode array spectrophotometer in a quartz cuvette having a path length of 1 cm at room temperature. The experiments were performed in the anaerobic chamber in 0.5× TNG buffer and pH 7.4. Proline NONOate stocks prepared in 10 mM NaOH was used as the source of NO. Thiol-reduced protein (~0.3 mM, 60 μL) was treated with 1 M dithionite (5.5 μL) for 30 min to reduce the ferric protein to Fe^{2+}. Attempts to carry out titrations in the presence of dithionite resulted in severe precipitation and the requirement for unreasonably high amounts of NO to reach saturation indicating an interaction between dithionite and NO. Hence, dithionite was removed from the protein by two consecutive buffer exchanges using Microbiospin6 columns. The buffer-exchanged protein was diluted to 3 mL for spectrophotometric titrations. Increasing amounts of NO were titrated to the protein solution and the absorption spectrum of the protein was monitored until the equilibrium was reached. The Proline NONOate stock concentration was determined by the absorption at 252 nm (ε = 8,400 $M^{-1} \cdot cm^{-1}$). The absorption of the Soret band maximum was plotted as a function of the concentration of NO (assuming one molecule of proline NONOate releases two molecules of NO) and the data obtained were fit to Eq. **3**,

$$A = A_0 + (A_m - A_0) \times \frac{([P]_t + [NO]_t + K_d) - \sqrt{([P]_t + [NO]_t + K_d)^2 - 4[P]_t[NO]_t}}{2 \times [P]_t}, \quad [3]$$

where A is the observed absorption of the protein–NO complex, A_0 is the absorption of the protein in absence of any NO, A_m is the absorption of the completely NO-bound protein, $[NO]_t$ is the total NO concentration, and $[P]_t$ is the protein concentration. $[P]_t$ in Eq. **3** was left as a variable, as the inflection point of the fit (representative of $[P]_t$) was sometimes lower than the known concentration of protein in the cuvette. K_d is reported as mean ± SD from five experiments.

EPR Spectroscopy. EPR spectra were recorded at 11 and 15 K on an X-band Bruker EMX spectrometer (Bruker Biospin Corp.) containing an Oxford ITC4 temperature controller. All EPR samples were prepared in 0.5× TNG buffer. The samples were frozen in liquid nitrogen before experiments. Care was taken to ensure the use of the same internal- and external-diameter quartz tubes for EPR experiments as well as the same volumes of the sample for quantification purposes.

EPR of the protein. EPR of the thiol-reduced protein was carried out to test the integrity of the protein as well as quantification purposes. Thiol-reduced protein was prepared as described previously. The EPR sample for the protein was prepared in the anaerobic chamber with <0.3 ppm dioxygen. The heme content of the protein was determined using the pyridine hemochrome assay.

Whole-cell EPR. Whole-cell EPR was carried out for the detection/quantification of the Fe^{3+}-LBD complex in cellulo. *E. coli* cells expressing the LBD were inoculated from a starter culture into a secondary culture. The secondary culture was grown in the presence of 25 μM heme (heme stocks were prepared in DMSO as described previously). The cells were harvested by centrifugation. The pellet obtained from a 1-L culture was resuspended in ~5 mL 0.5× TNG buffer and pH 7.4 or pH 8.0 depending on the experiment. The cell suspension was diluted two-fold, including treatments with all the chemicals, for the final EPR experiments. CORM-A1 (Sigma) and proline NONOate (Cayman chemicals) were used as sources of CO and NO respectively. CORM-A1 is a metal ion–independent CO-releasing molecule with a half-life of 21 min at 37 °C and pH 7.4. The chemical concentrations and times of incubation are indicated in the figure legend of Fig. 4. Primary stocks of CORM-A1 and proline NONOate were prepared in 10 mM NaOH. Treatment of *E. coli* cells with CORM-A1 and proline NONOate were carried out in sealed serum vials maintained at a temperature of 37 °C. Cell-samples were withdrawn from sealed vials at different time points for the time-

dependent studies of CORM treatment on *E. coli* cells. EPR acquisition parameters for individual samples/sets of experiments have been mentioned in the respective figure legend. CORM treatment also resulted in a decrease in the EPR signal intensity of the cellular Mn^{2+} complex (six-line spectra between 2970 G and 3655 G). Therefore, the ratio of the EPR intensity of the Fe^{3+} LBD normalized to cellular Mn^{2+} complexes was also calculated and depicted in *SI Appendix*, Fig. S7*B*.

Stocks of dithionite (1 M) and H_2O_2 (1 M) were prepared in 1 M Tris pH 8.0 and water, respectively.

Quantification of LBD-bound heme in whole cells. The percentage increase or decrease in the EPR signal observed in dithionite- and H_2O_2-treated cells has been reported based on the EPR signal intensity change at g_z (2.49) of the rhombic spectrum exhibited by the protein Fe^{3+}-heme.

CO Concentration Determination. CO concentration of the buffers/solutions was determined by titration against reduced equine Myoglobin (Sigma). Experiments were carried out in a sealed cuvette with minimum headspace for any gas exchange. The CO concentrations were estimated from the percentage conversion of Fe^{2+}-Myoglobin to Fe^{2+}-CO Myoglobin assuming stoichiometric binding to Myoglobin. The concentrations of Fe^{2+}-Myoglobin and Fe^{2+}-CO Myoglobin were determined from the absorption at 435 nm ($\varepsilon = 121\ mM^{-1} \cdot cm^{-1}$) and 424 nm ($\varepsilon = 207\ mM^{-1} \cdot cm^{-1}$), respectively. The concentration of CO in 0.5× TNG buffer was determined to be 439 μM.

Thermodynamic Box Calculations for CO/NO Binding to the Fe^{3+}-LBD. Derivation of the thermodynamic parameters for different equilibria depicted in the thermodynamic box in Fig. 3*A* for reaction of the Fe^{3+}-LBD with CO and NO are given below. [red] and [oxd] indicate the concentration of reduced and oxidized protein.

$Fe^{3+/2+}$ redox equilibrium.

$$Fe^{3+}LBD \rightleftharpoons Fe^{2+}LBD \quad [4]$$

Our redox titrations yield two populations of the proteins with E° values of −0.225 V and −0.405 V and relative amplitudes of 0.4136 and 0.5864, respectively (Table 1). The relative content of the reduced and oxidized forms for each population at a potential of −280 mV (which is the nuclear potential) (23) was calculated based on the Nernst Eq. **5**:

$$E = E^0 - 0.0591 log \frac{[red]}{[oxd]}. \quad [5]$$

Taking into account the amplitudes of each of these populations and the individual ratios of oxidized versus reduced protein, overall, 62.5% of the protein exists in the oxidized and 37.5% of the protein in the reduced form:

$$\frac{[oxd]}{[red]} = \frac{0.625}{0.375}. \quad [6]$$

$Fe^{3+/2+}$ redox equilibrium in the presence of CO/NO.

$$Fe^{3+} - CO/NO\ LBD \rightleftharpoons Fe^{2+} - CO/NO\ LBD. \quad [7]$$

Our redox titrations indicate the E° for Fe^{3+}-CO/Fe^{2+}-CO equilibrium > 989 mV and Fe^{3+}-NO/Fe^{2+}-NO equilibrium > 819 mV. The ratio of the reduced to oxidized protein in the presence of the gases at a potential of −280 mV calculated using Eq. **5** is

$$\frac{[red]}{[oxd]} > 3.16 \times 10^{21}$$

for CO and

$$\frac{[red]}{[oxd]} > 3.98 \times 10^{18} \quad [8]$$

for NO.

Therefore, for our redox reaction with CO (Fig. 2*B*) when the total concentration of Rev-Erbβ LBD protein was 95.5 μM, [oxd] < 3.02×10^{-20} μM and [red] ≅ 95.5 − 3.02×10^{-20} ≅ 95.5 μM.

Similarly, for redox titrations in presence of NO (Fig. 2*D*) when the total concentration of LBD protein was 99.1 μM, [oxd] < 2.49×10^{-18} μM and [red] ≅ 99.1 − 2.49×10^{-18} ≅ 99.1 μM.

Dissociation Constant of Fe^{3+}-CO/NO LBD.

$$Fe^{3+}LBD + CO/NO \rightleftharpoons Fe^{3+}LBD - CO/NO. \quad [9]$$

Dissociation constant, K_{d2}, for the above reaction is given by

$$K_{d2} = \frac{[Fe^{3+}LBD] \times [CO/NO]}{[Fe^{3+}LBD - CO/NO]}. \quad [10]$$

For the redox titrations in presence of CO, [Fe^{3+}LBD] ≅ 95.5 − 3.02×10^{-20} ≅ 95.5 μM; [CO] = 439 μM (see CO Concentration Determination); [Fe^{3+}LBD-CO] < 3.02×10^{-20} μM. Therefore, K_{d2} (in presence of CO) > 1.39×10^{18}M. For the redox titrations in presence of NO, [Fe^{3+}LBD] ≅ 99.1 − 2.49×10^{-18} ≅ 99.1 μM; [NO] = 1.94 mM (solubility of NO in water) (50); [Fe^{3+}LBD-NO] < 2.49×10^{-18} μM. Therefore, K_{d2} (in presence of NO) > 7.72×10^{16} M.

Control Experiments to Explain the Origin of 422 nm Soret Peak of the Reduced Protein. We performed a few control experiments to account for the serendipitous occurrence of the 422 nm Soret peak for the reduced protein: 1) Integrity of the Fe^{3+} protein was checked by EPR spectroscopy. The EPR indicated the absence of any form of LS or HS ferric heme other than the His/Cys-LS form (*SI Appendix*, Fig. S8). 2) The addition of dye mixture did not elicit any significant spectral change in the protein-eliminating nonspecific interaction of the ferric protein with dyes (*SI Appendix*, Fig. S9). 3) The chemical reduction of the protein (with dyes) using the dithionite yielded the reduced protein with Soret peak at 427 nm eliminating nonspecific interaction of the reduced protein with dyes (*SI Appendix*, Fig. S9). 4) The integrity of the CV-27 voltammogram was verified by using a multimeter in parallel to the electrode setup in the cuvette to reconfirm the values of applied potential.

Data Availability. All study data are included in the article and *SI Appendix*.

ACKNOWLEDGMENTS. CODH protein was kindly donated by Daniel Esckilsen, Ragsdale Laboratory, University of Michigan. We acknowledge the technical help received from Thomas Yavaraski, Department of Civil and Environmental Engineering, University of Michigan for the gas chromatography–mass spectrometry experiments. The funding for the research was supported by NIH Grant R01-GM123513 (to S.W.R.).

1. C. Crumbley, T. P. Burris, Direct regulation of CLOCK expression by REV-ERB. *PLoS One* **6**, e17290 (2011).
2. R. Ikeda *et al*., REV-ERBα and REV-ERBβ function as key factors regulating Mammalian Circadian Output. *Sci. Rep.* **9**, [10]171 (2019).
3. D. J. Kojetin, T. P. Burris, REV-ERB and ROR nuclear receptors as drug targets. *Nat. Rev. Drug Discov.* **13**, 197–216 (2014).
4. H. Cho *et al*., Regulation of circadian behaviour and metabolism by REV-ERB-α and REV-ERB-β. *Nature* **485**, 123–127 (2012).
5. P. Kumar Jha, E. Challet, A. Kalsbeek, Circadian rhythms in glucose and lipid metabolism in nocturnal and diurnal mammals. *Mol. Cell. Endocrinol.* **418**, 74–88 (2015).
6. A. Bugge *et al*., Rev-erbα and Rev-erbβ coordinately protect the circadian clock and normal metabolic function. *Genes Dev.* **26**, 657–667 (2012).
7. M. T. Lam *et al*., Rev-Erbs repress macrophage gene expression by inhibiting enhancer-directed transcription. *Nature* **498**, 511–515 (2013).
8. L. Yin *et al*., Rev-erbalpha, a heme sensor that coordinates metabolic and circadian pathways. *Science* **318**, 1786–1789 (2007).
9. J. E. Gibbs *et al*., The nuclear receptor REV-ERBα mediates circadian regulation of innate immunity through selective regulation of inflammatory cytokines. *Proc. Natl. Acad. Sci. U.S.A.* **109**, 582–587 (2012).
10. J. Jager *et al*., Behavioral changes and dopaminergic dysregulation in mice lacking the nuclear receptor Rev-erbα. *Mol. Endocrinol.* **28**, 490–498 (2014).
11. A. Schnell *et al*., The nuclear receptor REV-ERBα regulates Fabp7 and modulates adult hippocampal neurogenesis. *PLoS One* **9**, e99883 (2014).
12. P. Valnegri *et al*., A circadian clock in hippocampus is regulated by interaction between oligophrenin-1 and Rev-erbα. *Nat. Neurosci.* **14**, 1293–1301 (2011).
13. E. L. Carter, S. W. Ragsdale, Modulation of nuclear receptor function by cellular redox poise. *J. Inorg. Biochem.* **133**, 92–103 (2014).
14. E. L. Carter, N. Gupta, S. W. Ragsdale, High affinity heme binding to a heme regulatory motif on the nuclear receptor rev-erbβ leads to its degradation and indirectly regulates its interaction with nuclear receptor corepressor. *J. Biol. Chem.* **291**, 2196–2222 (2016).
15. E. L. Carter, Y. Ramirez, S. W. Ragsdale, The heme-regulatory motif of nuclear receptor Rev-erbβ is a key mediator of heme and redox signaling in circadian rhythm maintenance and metabolism. *J. Biol. Chem.* **292**, 11280–11299 (2017).
16. T. Shimizu *et al*., Gaseous O2, NO, and CO in signal transduction: Structure and function relationships of heme-based gas sensors and heme-redox sensors. *Chem. Rev.* **115**, 6491–6533 (2015).
17. K. A. Marvin *et al*., Nuclear receptors homo sapiens Rev-erbbeta and Drosophila melanogaster E75 are thiolate-ligated heme proteins which undergo redox-mediated ligand switching and bind CO and NO. *Biochemistry* **48**, 7056–7071 (2009).

18. K. I. Pardee *et al*., The structural basis of gas-responsive transcription by the human nuclear hormone receptor REV-ERBbeta. *PLoS Biol.* **7**, e43 (2009).
19. N. Gupta, S. W. Ragsdale, Thiol-disulfide redox dependence of heme binding and heme ligand switching in nuclear hormone receptor rev-erbbeta. *J. Biol. Chem.* **286**, 4392–4403 (2011).
20. D. A. Hanna *et al*., Heme dynamics and trafficking factors revealed by genetically encoded fluorescent heme sensors. *Proc. Natl. Acad. Sci. U.S.A.* **113**, 7539–7544 (2016).
21. L. Cáceres *et al*., Nitric oxide coordinates metabolism, growth, and development via the nuclear receptor E75. *Genes Dev.* **25**, 1476–1485 (2011).
22. J. Reinking *et al*., The Drosophila nuclear receptor e75 contains heme and is gas responsive. *Cell* **122**, 195–207 (2005).
23. Y. M. Go, D. P. Jones, Redox control systems in the nucleus: Mechanisms and functions. *Antioxid. Redox Signal.* **13**, 489–509 (2010).
24. E. A. Sweeny *et al*., Glyceraldehyde-3-phosphate dehydrogenase is a chaperone that allocates labile heme in cells. *J. Biol. Chem.* **293**, 14557–14568 (2018).
25. A. Galmozzi *et al*., PGRMC2 is an intracellular haem chaperone critical for adipocyte function. *Nature* **576**, 138–142 (2019).
26. F. H. Bach, Heme oxygenase-1 as a protective gene. *Wien. Klin. Wochenschr.* **114** (suppl. 4), 1–3 (2002).
27. M. Deponte, The incomplete Glutathione puzzle: Just guessing at numbers and figures? *Antioxid. Redox Signal.* **27**, 1130–1161 (2017).
28. P. Diaz-Vivancos, A. de Simone, G. Kiddle, C. H. Foyer, Glutathione–Linking cell proliferation to oxidative stress. *Free Radic. Biol. Med.* **89**, 1154–1164 (2015).
29. A. Scirè *et al*., Glutathione compartmentalization and its role in glutathionylation and other regulatory processes of cellular pathways. *Biofactors* **45**, 152–168 (2019).
30. I. S. Arts, A. Gennaris, J.-F. Collet, Reducing systems protecting the bacterial cell envelope from oxidative damage. *FEBS Lett.* **589**, 1559–1568 (2015).
31. H. Østergaard, A. Henriksen, F. G. Hansen, J. R. Winther, Shedding light on disulfide bond formation: Engineering a redox switch in green fluorescent protein. *EMBO J.* **20**, 5853–5862 (2001).
32. M. F. Taylor, M. H. Boylan, D. E. Edmondson, Azotobacter vinelandii flavodoxin: Purification and properties of the recombinant, dephospho form expressed in Escherichia coli. *Biochemistry* **29**, 6911–6918 (1990).
33. C. J. Reedy, M. M. Elvekrog, B. R. Gibney, Development of a heme protein structure-electrochemical function database. *Nucleic Acids Res.* **36**, D307–D313 (2008).
34. D. Bickar, C. Bonaventura, J. Bonaventura, Carbon monoxide-driven reduction of ferric heme and heme proteins. *J. Biol. Chem.* **259**, 10777–10783 (1984).
35. M. Can, F. A. Armstrong, S. W. Ragsdale, Structure, function, and mechanism of the nickel metalloenzymes, CO dehydrogenase, and acetyl-CoA synthase. *Chem. Rev.* **114**, 4149–4174 (2014).
36. S. Hirota, K. Azuma, M. Fukuba, S. Kuroiwa, N. Funasaki, Heme reduction by intramolecular electron transfer in cysteine mutant myoglobin under carbon monoxide atmosphere. *Biochemistry* **44**, 10322–10327 (2005).
37. P. C. Ford, B. O. Fernandez, M. D. Lim, Mechanisms of reductive nitrosylation in iron and copper models relevant to biological systems. *Chem. Rev.* **105**, 2439–2455 (2005).
38. C. E. Tinberg *et al*., Characterization of iron dinitrosyl species formed in the reaction of nitric oxide with a biological Rieske center. *J. Am. Chem. Soc.* **132**, 18168–18176 (2010).
39. S. Carballal *et al*., Kinetics of reversible reductive carbonylation of heme in human cystathionine β-synthase. *Biochemistry* **52**, 4553–4562 (2013).
40. S. Hammes-Schiffer, A. A. Stuchebrukhov, Theory of coupled electron and proton transfer reactions. *Chem. Rev.* **110**, 6939–6960 (2010).
41. N. G. Leferink *et al*., Gating mechanisms for biological electron transfer: Integrating structure with biophysics reveals the nature of redox control in cytochrome P450 reductase and copper-dependent nitrite reductase. *FEBS Lett.* **586**, 578–584 (2012).
42. W. A. Johnston *et al*., Cytochrome P450 is present in both ferrous and ferric forms in the resting state within intact Escherichia coli and hepatocytes. *J. Biol. Chem.* **286**, 40750–40759 (2011).
43. S. M. Kapetanaki *et al*., A mechanism for CO regulation of ion channels. *Nat. Commun.* **9**, 907 (2018).
44. H. Nakajima *et al*., Redox properties and coordination structure of the heme in the co-sensing transcriptional activator CooA. *J. Biol. Chem.* **276**, 7055–7061 (2001).
45. S. Carballal *et al*., Dioxygen reactivity and heme redox potential of truncated human cystathionine β-synthase. *Biochemistry* **47**, 3194–3201 (2008).
46. X. D. Ding *et al*., Nitric oxide binding to the ferri- and ferroheme states of nitrophorin 1, a reversible NO-binding heme protein from the saliva of the blood-sucking insect, Rhodnius prolixus. *J. Am. Chem. Soc.* **121**, 128–138 (1999).
47. I. Barr, F. Guo, Pyridine hemochromagen assay for determining the concentration of heme in purified protein solutions. *Bio Protoc.* **5**, e1594 (2015).
48. R. M. C. Dawson, D. C. Elliott, W. H. Elliott, K. M. Jones, *Data for Biochemical Research* (Clarendon Press, ed. 2, 1969).
49. R. F. Homer, T. E. Tomlinson, 504. The stereochemistry of the bridged quaternary salts of 2,2′-bipyridyl. *J. Chem. Soc.* 2498–2503 (1960).
50. I. G. Zacharia, W. M. Deen, Diffusivity and solubility of nitric oxide in water and saline. *Ann. Biomed. Eng.* **33**, 214–222 (2005).
51. I. Efimov *et al*., A simple method for the determination of reduction potentials in heme proteins. *FEBS Lett.* **588**, 701–704 (2014).
52. W. M. Clark, *Oxidation-Reduction Potentials of Organic Systems* (Robert E. Krieger Publishing Company, 1972).
53. R. T. Salmon, F. M. Hawkridge, The electrochemical properties of three dipyridinium salts as mediators. *J. Electroanal. Chem. Interfacial Electrochem.* **112**, 253–264 (1980).
54. P. Wardman, Reduction potentials of one-electron couples involving free radicals in aqueous solution. *J. Phys. Chem. Ref. Data* **18**, 1637–1755 (1989).
55. M. S. Chan, J. R. Bolton, Structures, reduction potentials and absorption maxima of synthetic dyes of interest in photochemical solar-energy storage studies. *Sol. Energy* **24**, 561–574 (1980).